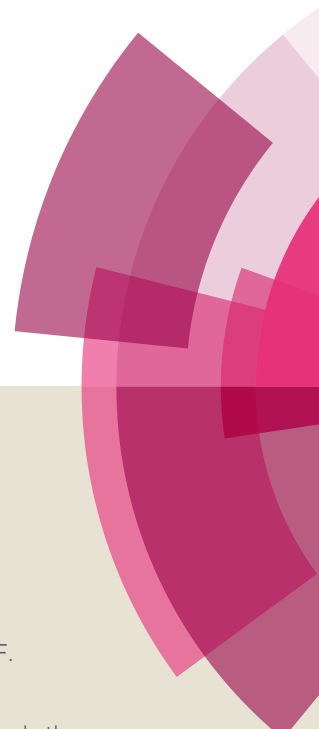


# NJC

Accepted Manuscript



This article can be cited before page numbers have been issued, to do this please use: J. Jiao, H. Wu, F. Chen, R. Chen, B. Sun and M. Wang, *New J. Chem.*, 2018, DOI: 10.1039/C8NJ00578H.



This is an Accepted Manuscript, which has been through the Royal Society of Chemistry peer review process and has been accepted for publication.

Accepted Manuscripts are published online shortly after acceptance, before technical editing, formatting and proof reading. Using this free service, authors can make their results available to the community, in citable form, before we publish the edited article. We will replace this Accepted Manuscript with the edited and formatted Advance Article as soon as it is available.

You can find more information about Accepted Manuscripts in the [author guidelines](#).

Please note that technical editing may introduce minor changes to the text and/or graphics, which may alter content. The journal's standard [Terms & Conditions](#) and the ethical guidelines, outlined in our [author and reviewer resource centre](#), still apply. In no event shall the Royal Society of Chemistry be held responsible for any errors or omissions in this Accepted Manuscript or any consequences arising from the use of any information it contains.

## Delivery of coumarin-containing all-trans retinoic acid derivative via targeted nanoparticles encapsulating indocyanine green for chemo/photothermal/photodynamic therapy of breast cancer

Jia Jiao<sup>a</sup>, Hongshuai Wu<sup>a</sup>, Fanghui Chen<sup>a</sup>, Renjie Chen<sup>b</sup>, Baiwang Sun<sup>a,\*</sup>,  
Mingliang Wang<sup>a,\*</sup>

<sup>a</sup> School of Chemistry and Chemical Engineering, Southeast University, Nanjing 210089, PR China. Fax: +86 25 52090614, Tel: +86 25 52090614, E-mail address: chmsunbw@seu.edu.cn

<sup>b</sup> Affiliated Hospital 2, Nanjing Medical University, Nanjing 210011, PR China

**Abstract:** Developing the chemo/photothermal/photodynamic therapy with nanoplatfroms offers a promising strategy for effective cancer treatment. Recently, all-trans retinoic acid (ATRA), as a potential antitumor drug, has drawn great attention in improving its antitumor activity. In this study, a novel coumarin-containing ATRA (AC) and indocyanine green (ICG) dye loaded nanoparticles, with the targeted ligand cyclic (Arg-Gly-Asp-D-Phe-Lys) (cRGD) peptide, were fabricated by self-assembling, as a new theranostic nanoplatfrom for chemo/photothermal/photodynamic therapy. The formed nanoparticles (AC/ICG-TNPs) had a diameter of around 133 nm with uniform monodispersity. Additionally, AC/ICG-TNPs showed marked stability under the normal physiological conditions. However, it could rapidly release drug under the mild acidic microenvironment. Moreover, confocal microscopy observations confirmed that the uptake of AC/ICG-TNPs increased in the breast cancer cells, especially in MDA-MB-231 cells, probably mediated by cRGD via specific recognition of the overexpressed integrin  $\alpha_v\beta_3$ . Meanwhile, free AC exhibited stronger cytotoxic effects than free ATRA in MTT assay, and AC/ICG-TNPs were demonstrated to possess the excellent antitumor efficacy when exposed to NIR irradiation through the combination therapy. Hence, this designed therapeutic method is a good candidate for the improved bioactivity of ATRA and the site-specific

combinational therapy against breast cancer.

**KEYWORDS:** nanoparticles, therapeutic efficacy, photothermal therapy, photodynamic therapy, ATRA, coumarin, active targeting

## 1. Introduction

Breast carcinoma is a devastating malignancy and represents the primary driver of cancer-related death among women worldwide.<sup>1,2</sup> At present, breast cancer treatments have been performed on the basis of clinical and pathologic staging and still far from optimal, which are mainly restricted to chemotherapy, radiation and surgery.<sup>3</sup> Recent decades have witnessed that nanotechnology provides a plethora of promising avenues for cancer therapy. The nanocarriers (liposomes, polymeric micelles, metal or oxide based nanoparticles), as an emerging class of therapeutics, can not only prolong plasma circulation time but also alleviate systemic toxicities and improve the water-solubility of hydrophobic small molecules.<sup>4-6</sup> In addition, the surface of nanocarriers functionalized with ligands can yield high affinity and specificity for target sites.<sup>7-9</sup> These significant features have drawn increasing interest in nanocarriers for improving therapeutic efficacy compared with the conventional chemotherapy.<sup>10-12</sup>

In both clinical practice and exploratory studies, it has been demonstrated that the monotherapy is inefficient to combat the tumor, which is mainly due to the reason that the subpopulations of cancer cells in heterogeneous tumor tissue have resistance to single treatment modality. Therefore, combination therapies with synergistic effect have obtained tremendous attention.<sup>5, 13, 14</sup> Indocyanine green (ICG), a near infrared dye, is able to simultaneously serve as a potential photosensitizer and photothermal conversion agent (PTCA) due to its capacity of generating reactive oxygen species (ROS) and the excellent photothermal conversion efficiency after irradiated by NIR laser.<sup>15</sup> Photothermal therapy (PTT) and photodynamic therapy (PDT), minimally invasive therapies, utilize the heat or ROS generated from the absorbed optical energy by photothermal conversion agents (PTCAs) or photosensitizers to damage malignant tumors.<sup>16</sup> Nevertheless, the limited tissue penetration of NIR light and the upregulated expression of heat shock protein in cancer cells greatly impede the performance of PTT and PDT. In view of these inadequacies, the combination of PTT, PDT and

chemotherapy is considered as an effective strategy to achieve the optimized performance.<sup>17</sup>

ATRA, the major active metabolite of vitamin A, participates in multiple biological processes, such as cell proliferation and differentiation.<sup>18</sup> ATRA has been shown to be potential work in prevention and treatment of cancers including breast cancer. Increasing evidence indicates that ATRA can block tumor growth through damaging tumor cell DNA and inhibiting tumor cell differentiation.<sup>19</sup> However, the utilization of ATRA is often hindered due to its limited toxicity and therapeutic efficacy. Consequently, many studies are focused on increasing its bioactivities via structural modification.<sup>20-24</sup> Coumarin, namely benzopyrone, is a versatile nucleus of various natural compounds with diverse physiological activities. It is reported that coumarin and its derivatives have anticancer activity against tumors including breast cancer.<sup>25-27</sup>

On the basis of the above, we synthesized a novel cytotoxic molecule, coumarin-containing all-trans retinoic acid derivative (AC), through linking ATRA with 7-hydroxy-4-trifluoromethyl coumarin (HTCM) by ester bond for the first time, which enhanced toxicity against tumor cells. Furthermore, AC and ICG were simultaneously loaded into one nanocarrier modified with cRGD peptide, one could effectively increase the accumulation of drugs in the breast cancer tumors, which overexpressed cell integrin  $\alpha_v\beta_3$ . And it is demonstrated that the designed nanoplatform could remarkably realize the synergistic effect of chemotherapy, PTT and PDT. All of the results indicated that the prepared nanosystem is a potential therapeutic strategy in clinical application for breast cancer therapy.

## 2. Materials and methods

### 2.1. Materials

DSPE-PEG<sub>2000</sub>-COOH, cRGD and ICG were purchased from Shanghai Pengshuo Biological technology Co., Ltd. (Shanghai, China). Resorcinol, ATRA, 2-(1H-Benzotriazole-1-yl)-1,1,3,3-tetramethyluronium tetrafluoroborate (TBTU), 4,4,4-Trifluoro-3-oxobutyric acid ethyl ester, 4-Methylmorpholine, 1-[3-(dimethylamino)propyl]-3-ethylcarbodiimide hydrochloride (EDCI) and N-hydroxysuccinimide (NHS) were bought from Aladdin Reagent Co. Ltd. (Shanghai,

China). Phosphate buffered saline (PBS), DMEM, RPMI1640 medium, sodium bicarbonate, penicillin-streptomycin antibiotics, fetal bovine serum (FBS), trypsin-EDTA and 3-(4,5-dimethylthiazol-2-yl)-2,5-diphenyltetrazolium bromide (MTT) were provided by Yucheng Biotechnology Co., Ltd. (Nanjing, China). 4',6-diamidino-2-phenylindole (DAPI), reactive oxygen species assay kit and Annexin V-FITC apoptosis detection kit were obtained from Sigma-Aldrich (St Louis, MO, USA). All other chemical reagents were purchased from Sinopharm Chemical Reagent Co., Ltd.

## 2.2. Preparation of AC/ICG-TNPs

In brief, DSPE-PEG<sub>2000</sub>-COOH (10mg), DSPE-PEG<sub>2000</sub>-cRGD (2mg), AC (2mg) and ICG (0.6 mg) were dissolved in dichloromethane (20 mL) and then the solvent evaporated under reduced pressure to form a thin film. After 10 mL of deionized water added into the mixture, the solution became suspension gradually as the formation of nanoparticles under sonication for 8 min via an ultrasonic processor. To remove unencapsulated drug molecules, the suspension was centrifuged at 3000 rpm and then filtrated with 0.22  $\mu$ m filter membrane. The nanoparticles was obtained by lyophilization and finally stored at 4 °C for further use. To serve as control, other nanoparticles including non-targeted nanoparticles encapsulating AC and ICG (AC/ICG-NPs), targeted nanoparticles without encapsulating AC (ICG-TNPs) and empty nanoparticles with or without targeted ligand (TNPs or NPs), were all prepared through the similar process.

## 2.3. Characterization of nanoparticles

The size and polydispersity (PDI) of nanoparticles were estimated by Dynamic Light Scattering (DLS). Briefly, the prepared nanoparticles were analyzed by a Brookhaven A8530 apparatus in triplicate at room temperature and the data were analyzed using Brookhaven Dispersion Technology Software. The zeta potential was detected by a Malvern Zetasizer Nanoseries (Malvern Instruments Zen 3600, Malvern, U.K.) and calculated using Brookhaven Dispersion Technology Software. The surface morphology of nanoparticles was further investigated by JEM-100CXII transmission electron microscopy (TEM). The samples were prepared for TEM by evaporating

water under weak light irradiation after dropped on a copper grid coated with carbon.

#### 2.4. Entrapment efficiency (EE) and drug loading capacity (DLC)

The EE and DLC of AC and ICG loaded in nanoparticles were measured by UV-vis spectrometer (UV-2450, Shimadzu, Japan) using a standard curve method as previously described.<sup>12, 28</sup> The entrapment efficiency and drug loading capacity were calculated according to the following equations:

$$EE (\%, AC \text{ or } ICG) = \frac{\text{Weight of drug in nanoparticles}}{\text{Weight of feeding drug}} \times 100\%$$

$$DLC (\%, AC \text{ or } ICG) = \frac{\text{Weight of drug in nanoparticles}}{\text{Weight of total drug loaded nanoparticles}} \times 100\%$$

#### 2.5. Stability of nanoparticles

The AC/ICG-TNPs were selected to be kept at 4 °C for up to 28 days. The stability of nanoparticles was detected by Dynamic Light Scattering (DLS) and UV-vis spectrometer on day 0, 7, 14, 21 and 28 to monitor the changes in size, PDI and UV absorption of nanoparticles. At each point in time, the suspended nanoparticles were centrifuged at 3000 RCF for 10 min to ensure that the impurities could be sedimented and then took out the certain volume of supernate to measure.

To further investigate the stability of AC/ICG-TNPs under physiological conditions, the prepared nanoparticles were evaluated by DLS in PBS with the presence of 10% FBS at different times.

#### 2.6. Drug release

The triggered release behaviors of AC from nanoparticles were studied at different physiological pH through the dialysis method.<sup>9</sup> Briefly, the prepared nanoparticles were dispersed in phosphate buffer (3.0 mL, pH 5.0, 6.0 or 7.4) and the suspension was placed into a dialysis bag (MWCO = 3500 Da). Then the dialysis bag was immersed in buffer medium at pH 5.0, 6.0 or 7.4, and gently shaken at 37 °C. At a preselected time, the dialysate (2 mL) was withdrawn to determine the amount of released drug utilizing UV-vis spectroscopy through comparing the absorption curve of pure AC, while a same amount (2 mL) of fresh buffer medium was added back to compensate the volume loss. Each sample was tested three times.

#### 2.7. Evaluation of photothermal conversion efficiency

The nanoparticle suspensions diluted to various concentrations (40  $\mu\text{g/mL}$ , 60  $\mu\text{g/mL}$ , 80  $\mu\text{g/mL}$  or 100  $\mu\text{g/mL}$ ) were exposed to 808 nm laser with a power of 1.5  $\text{W/cm}^2$  for 5 min. The changes of temperature of ICG mediated nanoparticles were recorded by thermal imager.

### 2.8. Cell culture

The human breast cancer cells MCF-7 cultured in RPMI 1640 medium and MDA-MB-231 maintained in DMEM were purchased from the Cell Bank of the Chinese Academy of Sciences (Shanghai, China). Both media were supplemented with 10% heat-inactivated fetal bovine serum (FBS) and 1% penicillin-streptomycin solution. The entire cells were cultured in a humidified atmosphere containing 5%  $\text{CO}_2$  at 37  $^\circ\text{C}$ .

### 2.9. Cellular uptake study

MCF-7 or MDA-MB-231 cells were seeded in the confocal petri dish at a density of  $2.0 \times 10^5$  cells per dish allowed to adhere for 24 h under 5%  $\text{CO}_2$  atmosphere at 37  $^\circ\text{C}$ . After the culture medium removed, the cells were washed three times with PBS. Then an appropriate amount of AC/ICG-TNPs or AC/ICG-NPs suspension with the same concentration of ICG was added into the cell culture medium and further incubation for different time durations (1, 4 or 12 h). After the cells fixed by 4% paraformaldehyde for 30 min at 37  $^\circ\text{C}$ , DAPI was added and the cells were stained for 15 min. Finally, the resulting samples were visualized with Confocal Laser Scanning Microscopic (CLSM).

### 2.10. Intracellular ROS Detection

The generation of intracellular ROS from AC/ICG-TNPs uptake by MDA-MB-231 cells after NIR laser irradiation were monitored with DCFH-DA probe. MDA-MB-231 cells were seeded in a 6-well plate at  $1 \times 10^5$  cells per well for 24 h and subsequently incubated with AC/ICG-TNPs for 12h. After removing the medium with nanoparticles, the cells were washed three times with PBS and incubated with DCFH-DA for another 20 min. Then the cells were washed with PBS and irradiated with 808 nm laser ( $1.5 \text{ W/cm}^2$ ) for 5 min. The fluorescence images were obtained using a confocal microscopy with 488 nm excitation and emission of 520 nm. ROS

generated in cells were also quantitatively measured by flow cytometry on a FACS Calibur (BD Biosciences, USA).

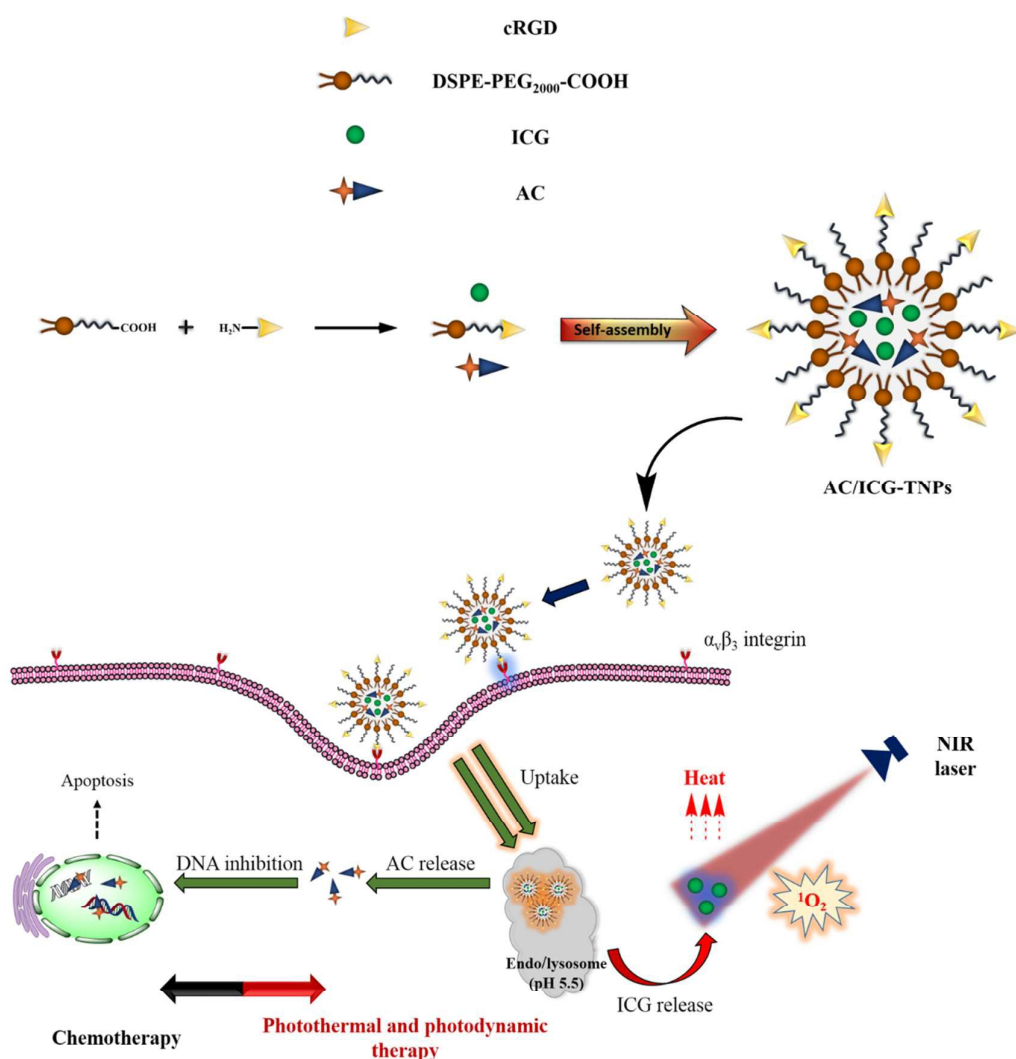
### 2.11. Cytotoxicity assays

Cytotoxicity of AC/ICG-TNPs was evaluated on MCF-7 and MDA-MB-231 cells by the MTT colorimetric method<sup>29</sup>. In brief, the cells were seeded in a 96-well plate with the density of  $1 \times 10^4$  cells per well. 24 h post-seeding, the cells were treated with various concentrations of the prepared nanoparticles. After incubation for 12 h, the medium was replaced with fresh one and the cells were then irradiated with 808 nm laser ( $1.5 \text{ W/cm}^2$ ) for 5 min. The cells were further cultured by 12 h at  $37 \text{ }^\circ\text{C}$ . Thereafter, 150  $\mu\text{L}$  of MTT solution (5 mg/mL) was added into each well and incubated for another 4 h. Afterward, the medium was replaced by 150  $\mu\text{L}$  of DMSO to dissolve the purple formazan and the absorbance at 490 nm was measured by a microplate reader. The cytotoxicity assay was performed thrice and the average value was taken from the three measurements.

### 2.12. Cell apoptosis

MCF-7 or MDA-MB-231 cells were seeded in the 6-well plate at  $1 \times 10^5$  cells per well and cultured for 24 h in an incubator. Then the cells were exposed to different concentrations of the prepared nanoparticles and incubated for 12 h, while the cells without treatment were used as a control. The complete medium was then replaced with fresh one and the cells were irradiated with 808 nm laser ( $1.5 \text{ W/cm}^2$ ) for 5 min. After that, the cells were cultured for additional 12 h. Both floating and attached cells were collected and washed thrice with PBS for quantitative measurement of apoptosis. After that, the cells were stained with Annexin V-FITC (5  $\mu\text{L}$ ) and propidium iodide (3  $\mu\text{L}$ ) for 15 min without light. Finally, the samples were analyzed by flow cytometry on a FACS Calibur (BD Biosciences, USA).

## 3. Results and discussion



**Scheme 1.** Schematic illustration of AC/ICG-TNPs for targeted and chemo/photothermal/photodynamic therapy.

### 3.1. Preparation and characterization of nanoparticles

In this study, several forms of nanoparticles were prepared through thin-film hydration method under sterile conditions. The schematic diagram of preparation process was presented in **Scheme 1**. As depicted in **Figure 1A**, the suspension of TNPs exhibited colorless, while the ICG-TNPs and AC/ICG-TNPs suspension displayed green and yellow green colors, respectively, which demonstrated ICG and AC were encapsulated successfully. And the AC/ICG-TNPs suspensions presented evident Tyndall phenomenon. Obviously, the absorption spectrum of AC/ICG-TNPs

showed a blue-shifted absorption peak of AC from 373 nm to 326 nm (**Figure 1A**, **Figure S6A**). Meanwhile, the absorption spectrum exhibited a peak at 792 nm, which was attributed to the ICG content (**Figure 1A**).

The surface morphology, size and size distribution of the nanoparticles were investigated by TEM and DLS (**Figure 1B**, **Figure 1C**, **Table 1**). It was noticed that the average diameter of AC/ICG-TNPs was around 133 nm with almost regular spherical morphology and good monodispersity. Moreover, the size had no significant difference between NPs and TNPs, while the size of AC/ICG-TNPs is slightly larger than that of TNPs. The increase of nanoparticle size should be attributed to the successful encapsulation of AC and ICG and the results were consistent with the statistical charts inseted in TEM images (**Figure 1C**). It was reported that nanoparticles with a size 30-200 nm could favorably accumulate in cancer tissues via EPR.<sup>11, 30</sup> Therefore, the prepared AC/ICG-TNPs had the potential of enhanced accumulation in tumor sites. The tested results for the zeta potential demonstrated that after the introduction of targeting ligand cRGD peptide into nanoparticles, the surface charge of nanoparticles significantly increased from -40.2 mV to -22.9 mV (**Figure 1D**, **Figure S6**, **Figure S6F**). This phenomenon might result from the presence of positively charged amide and guanidine groups in cRGD peptide.

UV-vis absorption spectra and DLS of nanoparticles in phosphate buffer at pH 7.4 are shown in **Figure 1E** and **Figure 1F** to prove the stability of nanoparticles. After stored at 4 °C for four weeks, the suspension of AC/ICG-TNPs remained clear without obvious precipitation and the PDI parameters kept at a favorable level. Additionally, the particle size and the value of UV absorption peak showed little change. To further confirm the stability of the AC/ICG-TNPs under physiological conditions, the nanoparticles were measured by DLS in PBS with the presence of 10% FBS at 37 °C.<sup>15</sup> As shown in **Figure 2A**, the PDI remained below 0.3 and the size kept stable. These results suggested that the AC/ICG-TNPs would remain excellent stability under physiological conditions and may be used in the bloodstream with a long circulation time.

UV-vis spectroscopy was used for quantitative analysis of the content of ICG and

AC. As shown in **Table 1**, the AC/ICG-TNPs exhibited higher entrapment efficiency of ICG than AC, which should be due to the different form of drug-carried. Moreover, after the conjugation of cRGD peptide, EE and DLC had no obvious changes.

**Table 1.** Characteristics of AC/ICG-TNPs compared with AC/ICG-NPs.

NPs	Size (nm)	PDI	EE%/DLC% (AC)	EE%/DLC% (ICG)	Zeta potential (mV)
AC/ICG-NPs	127.89	0.238	34.36/6.64	71.84/4.09	-40.2
AC/ICG-TNPs	133.04	0.277	34.90/6.82	72.69/4.26	-22.9

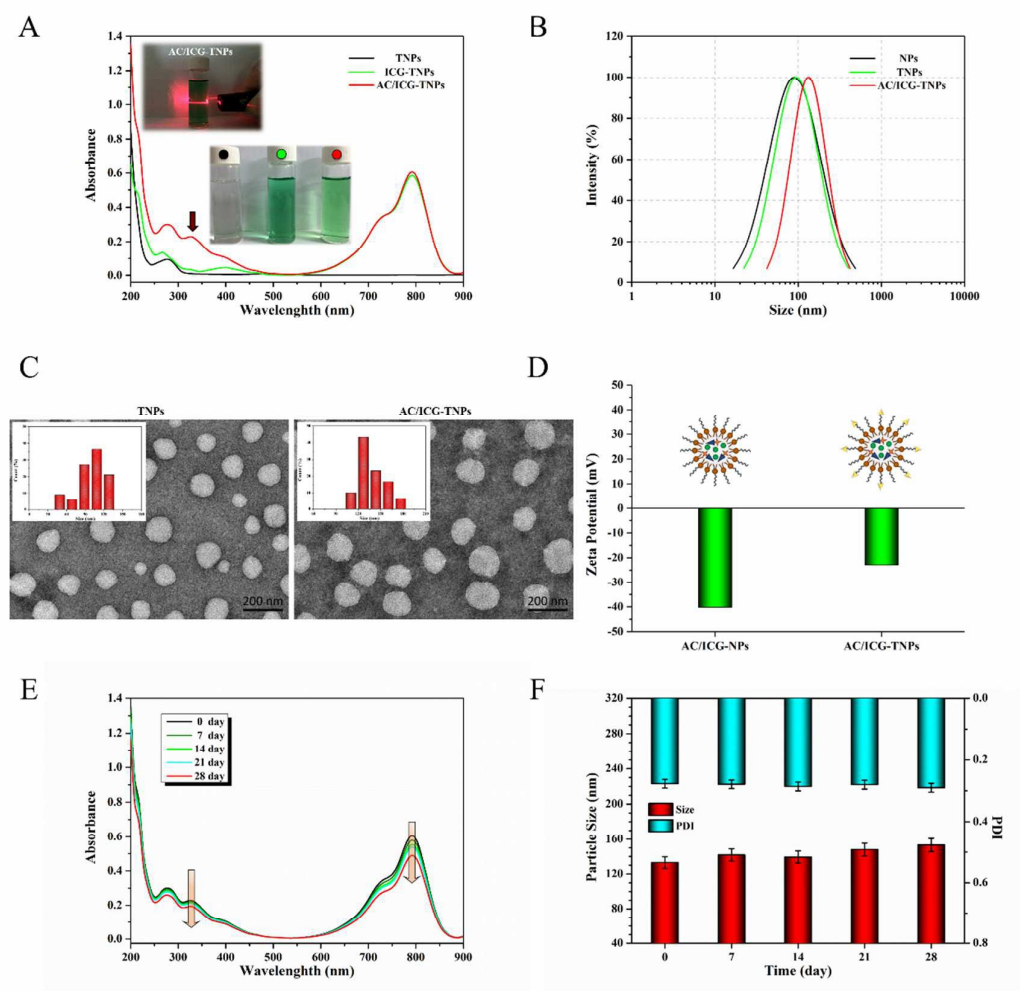


**Figure 1.** (A) UV-vis spectroscopy of TNPs, ICG-TNPs and AC/ICG-TNPs suspensions in phosphate buffer (pH 7.4). Inserted images are Tyndall phenomenon of AC/ICG-TNPs and the appearance of TNPs, ICG-TNPs AC/ICG-TNPs. (B) Size distribution of NPs, TNPs and AC/ICG-TNPs. (C) TEM images of TNPs and AC/ICG-TNPs. (D) Zeta potential of AC/ICG-NPs and AC/ICG-TNPs. (E) Changes

in UV-vis spectroscopy of AC/ICG-TNPs stored at 4 °C in phosphate buffer (pH 7.4) for 4 weeks. (F) Changes in size and PDI of AC/ICG-TNPs stored at 4 °C in phosphate buffer (pH 7.4) for 4 weeks.

### 3.2. Photothermal performance and in vitro release

To evaluate the photothermal efficiency, the AC/ICG-TNPs dispersed in water at different concentrations were irradiated by 808 nm laser at a power density of 1.5 W/cm<sup>2</sup> for 5 minutes, and water was treated as control. As shown in **Figure 2**, the temperature changes of AC/ICG-TNPs suspensions with various concentrations were monitored and recorded by thermal imager at certain exposed time interval. It was noticed that the increase of temperature in pure water under the NIR irradiation was almost negligible, while the AC/ICG-TNPs suspensions revealed an evident concentration-dependent temperature increase. The fastest and greatest temperature increase was obtained at the highest concentration of AC/ICG-TNPs (100 μg/mL), of which the temperature increased by 48 °C after 5 minutes of irradiation. These results obtained demonstrated the perfect photothermal conversion capacity mediated by ICG. It is known that the rapid temperature increase can confer irreversible thermal injury to cancer cells.

The standard curves of AC and ICG were measured with UV-vis spectroscopy (**Figure S6**). At 37 °C, dialysis was used to investigate the release efficiency of AC from the AC/ICG-TNPs when the pH was 6.0 or 5.0 and the physiological condition of pH 7.4 was used as the control. As displayed in **Figure 2D**, the release of AC were less than 20% after continuous incubation for 48 h at pH 7.4, which further proved the favorable structural stability and drug loading stability. In contrast, at slightly acidic conditions of pH 5.0 and 6.0, the corresponding percentages of released AC were up to approximately 84% and 70% after the same time, respectively. These results indicated that the AC/ICG-TNPs were relatively stable at physiological pH and also capable of the accelerated release of AC under the mild acidic condition. Specifically, the amounts of released AC increased along with a reduction in the pH value, which might be ascribed to the faster and more thorough disassembly of AC/ICG-TNPs at some degree in an acidic environment.<sup>30</sup> Thus, the accelerated release of drugs at

lower pH are preferable for the delivery of anticancer drugs.<sup>29, 31</sup>

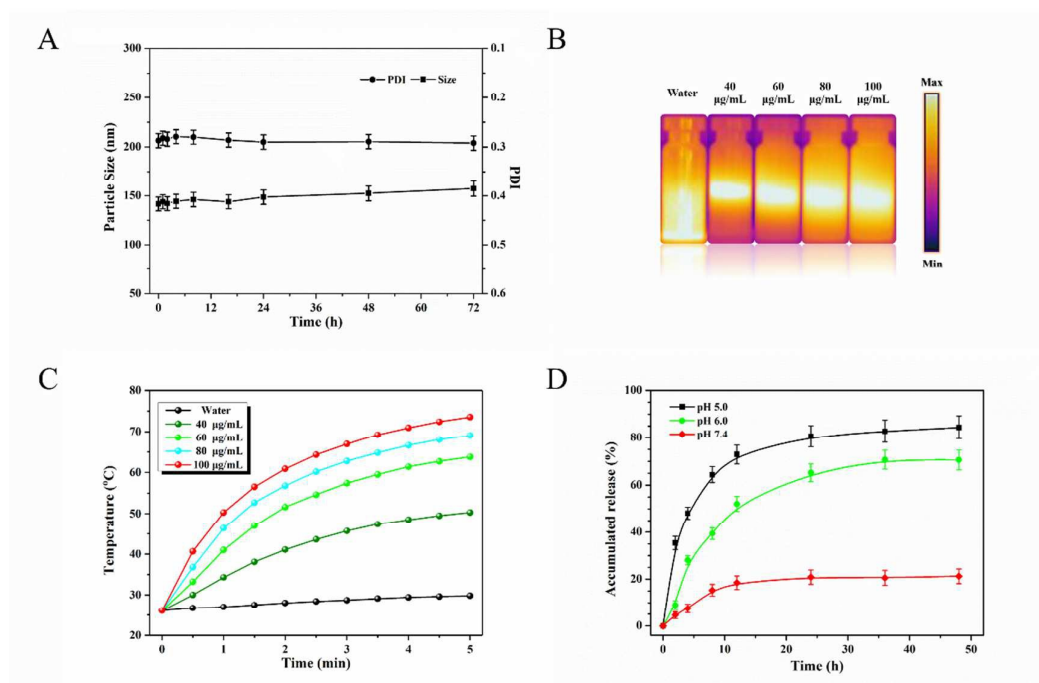


**Figure 2.** (A) Serum stability (against 10% FBS) of AC/ICG-TNPs in PBS at 37 °C. (B) Thermal imaging images of AC/ICG-TNPs detected by Infrared Camera. (C) Heating curves of water and various concentrations of AC/ICG-TNPs suspensions. (D) In vitro AC release profiles of AC/ICG-TNPs in pH 5.0, 6.0 and 7.4 at 37 °C.

### 3.3. Cell Internalization

Delivering therapeutic agents efficiently into tumor cells is crucial for the successful cancer therapy. Therefore, the cellular uptake of AC/ICG-NPs and AC/ICG-TNPs were investigated in MCF-7 and MDA-MB-231 cells using confocal laser scanning microscopy based on the red fluorescence of ICG. As shown in **Figure 3** and **Figure 4**, it was apparent that the representative red fluorescence was localized in the cytoplasm and nucleic regions of two cell lines at the 12-hour time-point and the internalization was found to be time-dependent. Meanwhile, the AC/ICG-TNPs exhibited stronger red fluorescence at any time-point in MDA-MB-231 cells compared to AC/ICG-NPs, but it could not observe these significant differences in MCF-7 cells. These phenomena suggested that the uptake of AC/ICG-TNPs could be closely related to the interaction of cRGD peptide with the overexpressed  $\alpha_v\beta_3$  integrin of MDA-MB-231 cells, while the weaker uptake efficiency of MCF-7 cells

was attributed to its low expression of  $\alpha_v\beta_3$ .<sup>32-34</sup> Interestingly, the AC/ICG-TNPs was also observed in the proximity of the nuclei and nuclei of MDA-MB-231 cells as shown by the red fluorescence in merged CLMS images (**Figure 4**), which was probably due to the localization of AC/ICG-TNPs or delivery of dye following endosomal/lysosomal escape.<sup>35</sup> Therefore, the above results demonstrated that the prepared nanoparticles possessed the potential to effectively improve the delivery and distribution of the drug in cancer cells.

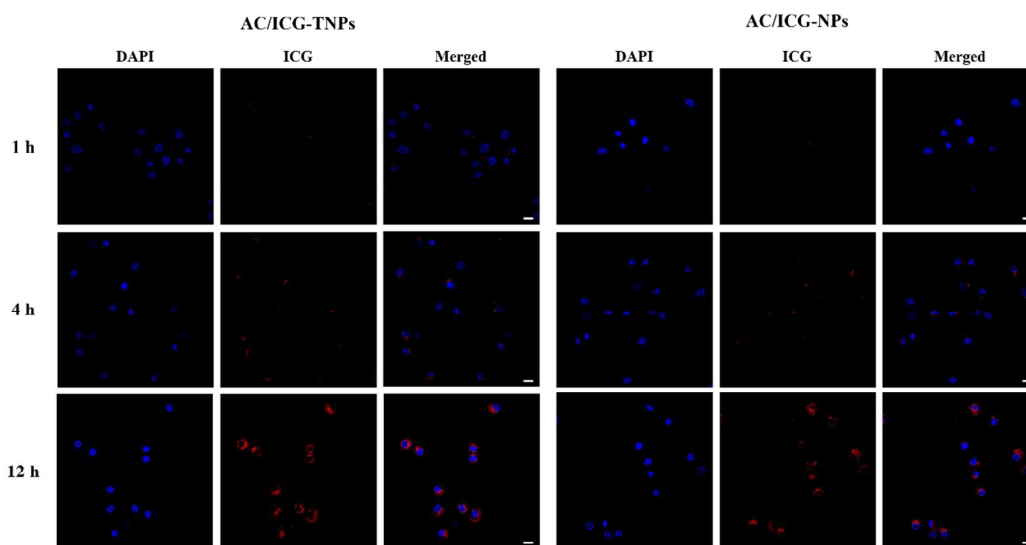


**Figure 3.** Confocal laser scanning microscopic images of cellular uptake in MCF-7 cells cultured with AC/ICG-TNPs and AC/ICG-NPs for different period time. Nuclei of cells stained with DPAI (blue) and ICG fluorescence in cells (red). Scale bar: 20  $\mu\text{m}$ .

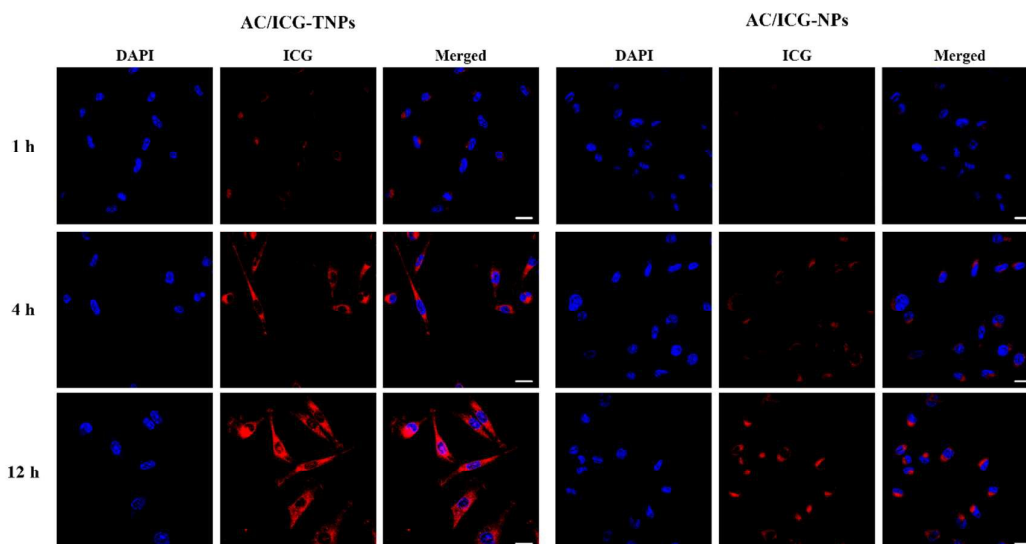


**Figure 4.** Confocal laser scanning microscopic images of cellular uptake in MDA-MB-231 cells cultured with AC/ICG-TNPs and AC/ICG-NPs for different period of time. Nuclei of cells stained with DPAI (blue) and ICG fluorescence in cells (red). Scale bar: 20  $\mu\text{m}$ .

### 3.4. Photodynamic performance

To prove AC/ICG-TNPs as the PDT agent, the DCFH-DA method was applied to detect the intracellular ROS of MDA-MB-231 with AC/ICG-TNPs under NIR laser irradiation. As shown in **Figure 5A**, in groups where MDA-MB-231 cells treated with AC/ICG-TNPs for 12 h and followed by being exposed to NIR laser irradiation, an intensive green fluorescence signal was detected. In contrast, the fluorescence signal were not significant for the control with laser or free AC with laser or AC/ICG-TNPs group. These results suggested the perfect capability of AC/ICG-TNPs mediated by ICG with NIR irradiation in producing ROS. As depicted in **Figure 5B**, the quantification of induced ROS intensity was evaluated by flow cytometry. The fluorescence intensity for the AC/ICG-TNPs with NIR laser irradiation group was highest than that for the other three groups and there was no obvious difference in fluorescence intensity for the other three groups, which further confirmed the perfect capability of AC/ICG-TNPs mediated by ICG with NIR irradiation in generating ROS. These phenomena indicated that abundant ROS can be generated by AC/ICG-TNPs in MDA-MB-231 cells with NIR laser irradiation. Therefore, the ICG-mediated

AC/ICG-TNPs with NIR laser irradiation are suitable candidates in PDT.

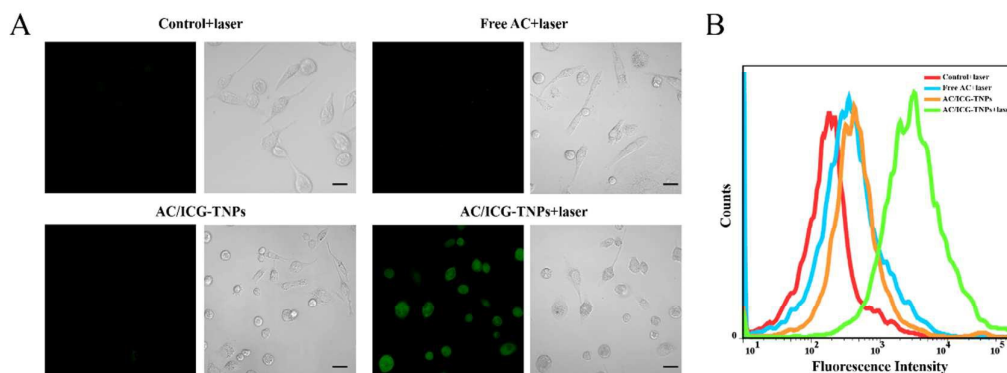


**Figure 5.** (A) CLSM images of singlet oxygen generation in MDA-MB-231 cells following various treatments as indicated. Green: ROS indicator DCFH-DA; scale bar: 20  $\mu\text{m}$ . (B) Quantification of induced ROS intensity achieved by flow cytometry.

### 3.5. In vitro cytotoxicity

We investigated the in vitro anticancer effects of the prepared nanoparticles using MCF-7 and MDA-MB-231 cells by MTT assay. For this purpose, both cell lines were treated with ATRA, AC, AC/ICG-TNPs and AC/ICG-TNPs with irradiation at concentrations ranging from 10  $\mu\text{M}$  to 120  $\mu\text{M}$ . As shown in **Figure 6**, the cytotoxicity of two kinds of free drugs and AC/ICG-TNPs all exhibited concentration-dependent profiles in two cell lines. AC displayed the stronger cytotoxic effects on MCF-7 and MDA-MB-231 cells especially at high concentrations compared to free ATRA, revealing that utilizing 7-hydroxy-4-trifluoromethyl coumarin to modify the structure of ATRA could obviously improve its antitumor effects. Meanwhile, the cell suppression capacity of AC/ICG-TNPs was slightly weaker than free AC even if the concentration was up to 120  $\mu\text{M}$ . It might be due to that AC easily diffused through the cellular membrane and quickly killing the malignant cells, while the nanoparticles released AC relatively slowly and resulted in the lower cytotoxicity at the same time.<sup>36</sup> However, AC/ICG-TNPs showed the stronger antitumor efficacy and even more approximately to free AC effect in MDA-MB-231 than that in MCF-7, which could be attributed to the higher expression levels of integrin  $\alpha_v\beta_3$  in MDA-MB-231 cells than in MCF-7 cells.<sup>32</sup> These results were also consistent with the cellular uptake study. Furthermore, the cell viability of

AC/ICG-TNPs under laser irradiation was the lowest among all the groups even achieving about 3.16% in MDA-MB-231 cells when the concentration was 120  $\mu\text{M}$  equivalent of AC, suggesting that the chemo/photothermal/photodynamic therapy provided by AC/ICG-TNPs were highly effective to the breast cancer cells, especially against MDA-MB-231 cells.

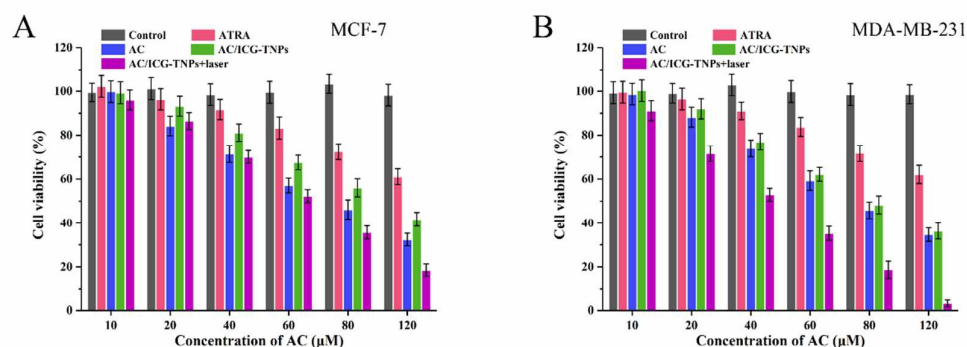


**Figure 6.** In vitro cytotoxicity of free ATRA, free AC, AC/ICG-TNPs and AC/ICG-TNPs with the laser irradiation (808 nm, 1.5 W/cm<sup>2</sup>) for 5 min against MCF-7 cells (A) and MDA-MB-231 cells (B).

### 3.6. Cell apoptosis

To further confirm that AC/ICG-TNPs with NIR laser irradiation could induce cell apoptosis for improving antitumor activity, the annexin V-FITC/PI assays were employed to analyze early and late apoptosis in MDA-MB-231 cells. As displayed in **Figure 7**, the control group with or without NIR laser irradiation both showed no obvious apoptosis rate (7.8% and 5.83%, respectively), which indicated that the laser irradiation exhibited negligible influence on MDA-MB-231 cells. Similarly, as for AC group, the laser irradiation also generated a slight impact on apoptosis rates. Nevertheless, AC/ICG-TNPs with laser irradiation induced 57.38% cell apoptosis, while the apoptosis rate was only 36.71% when the MDA-MB-231 cells cultivated with AC/ICG-TNPs without NIR irradiation. The remarkable elevated apoptosis rates further demonstrated the significant photothermal and photodynamic damage on MDA-MB-231 cells. Meanwhile, the apoptosis rate of AC was slightly higher than that of AC/ICG-TNPs, which was consistent with the results of the MTT assay. The apoptosis analysis data suggested that the AC/ICG-TNPs under NIR irradiation were a

promising and effective strategy to induce the apoptosis of MDA-MB-231 cells.

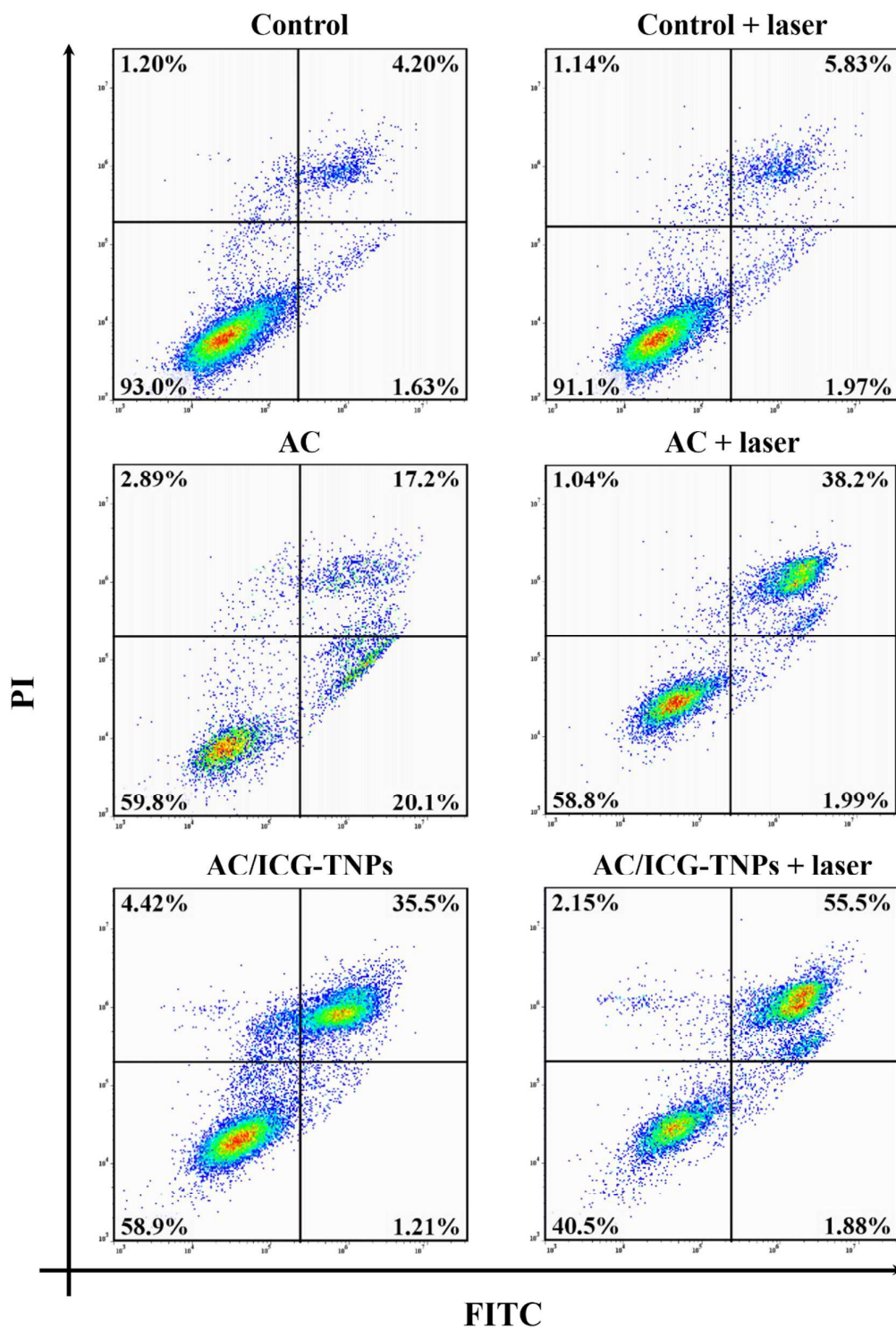


**Figure 7.** Cell apoptosis of MDA-MB-231 cells after incubation with free AC and AC/ICG-TNPs at an equivalent AC concentration of 60  $\mu$ M with or without NIR

irradiation.

#### 4. Conclusions

In summary, a novel anticancer drug AC was synthesized by conjugating ATRA with HTCM for enhancing the drug toxicity of ATRA. Then an active targeted AC-loaded nanoparticles encapsulating ICG dye was designed and prepared as the vehicle for chemo/photothermal/photodynamic therapy. DLS and TEM showed that the formed AC/ICG-TNPs had an appropriate diameter with uniform monodispersity. In addition, it was demonstrated that AC/ICG-TNPs could release AC rapidly under the mild acidic microenvironment, but it possessed good stability under the normal physiological conditions. Meanwhile, the encapsulated ICG dye could efficiently convert the NIR light into heat and generate ROS to accomplish the photothermal/photodynamic therapy upon NIR irradiation. On the basis of the active targeting mediated by overexpressed integrin  $\alpha_v\beta_3$  on the breast cancer cells MDA-MB-231, AC/ICG-TNPs could accumulate in tumor sites with high efficiency and achieve the enhanced cellular uptake. Thus it exhibited the obvious inhibition for cancer cells compared with AC/ICG-NPs. Furthermore, the cell apoptosis study testified that AC/ICG-TNPs showed more effective antitumor performance against the breast cancer cells after NIR irradiation due to chemo/photothermal/photodynamic therapy, which was consistent with the results of MTT assay. Taken together, the present results might afford a promising approach for the improved bioactivity of ATRA and the site-specific combinational antitumor therapy.

#### Conflicts of interest

There are no conflicts to declare.

#### Acknowledgements

This work was financially supported by the National Natural Science Foundation of China (Grant Nos. 21628101 and 21371031), the International S&T Cooperation Program of China (No. 2015DFG42240), the Priority Academic Program Development (PAPD) of Jiangsu Higher Education Institutions and the Technological Program Foundation of Jiangsu Province (No. BY2015070-09).

#### References

1. C. Q. Wang, C. H. Tang, Y. Wang, L. Jin, Q. Wang, X. Li, G. N. Hu, B. F. Huang, Y. M. Zhao and C. M. Su, *Scientific reports*, 2017, **7**, 15887.
2. R. Zhang, S.-B. Wang, W.-G. Wu, R. K. Kankala, A.-Z. Chen, Y.-G. Liu and J.-Q. Fan, *Journal of Nanoparticle Research*, 2017, **19**.
3. R. Misra, S. Acharya and S. K. Sahoo, *Drug discovery today*, 2010, **15**, 842-850.
4. M. Overchuk and G. Zheng, *Biomaterials*, 2017, **156**, 217-237.
5. W. Fan, B. Yung, P. Huang and X. Chen, *Chemical reviews*, 2017, **117**, 13566-13638.
6. T. Shi, L. Gu, Y. Sun, S. Wang, X. Zhang, J. Zhu and B. Sun, *European Polymer Journal*, 2017, **92**, 105-116.
7. M. L. Leite, N. B. da Cunha and F. F. Costa, *Pharmacology & therapeutics*, 2017, DOI: 10.1016/j.pharmthera.2017.10.010.
8. T. Shi, L. Gu, Y. Sun, S. Wang, C. You, X. Zhang, J. Zhu and B. Sun, *European journal of pharmacology*, 2017, **794**, 184-192.
9. C. You, H. Wu, M. Wang, Z. Gao, X. Zhang and B. Sun, *Nanotechnology*, 2018, **29**, 015601.
10. D. Wang, B. Liu, Y. Ma, C. Wu, Q. Mou, H. Deng, R. Wang, D. Yan, C. Zhang and X. Zhu, *Journal of the American Chemical Society*, 2017, **139**, 14021-14024.
11. C. You, H. Wu, M. Wang, Y. Zhang, J. Wang, Y. Luo, L. Zhai, B. Sun, X. Zhang and J. Zhu, *Chemistry*, 2017, **23**, 5352-5360.
12. C. You, J. Yu, Y. Sun, Y. Luo, X. Zhang, J. Zhu and B. Sun, *New Journal of Chemistry*, 2017, **41**, 773-785.
13. C. Gao, X. Liang, S. Mo, N. Zhang, D. Sun and Z. Dai, *ACS applied materials & interfaces*, 2018, DOI: 10.1021/acsami.7b14125.
14. S. M. Ardekani, A. Dehghani, M. Hassan, M. Kianinia, I. Aharonovich and V. G. Gomes, *Chemical Engineering Journal*, 2017, **330**, 651-662.
15. Y. Zhang, C. Teh, M. Li, C. Y. Ang, S. Y. Tan, Q. Qu, V. Korzh and Y. Zhao, *Chemistry of Materials*, 2016, **28**, 7039-7050.
16. J. C. Yang, Y. Chen, Y. H. Li and X. B. Yin, *ACS applied materials & interfaces*, 2017, **9**, 22278-22288.
17. L. Du, H. Qin, T. Ma, T. Zhang and D. Xing, *ACS nano*, 2017, **11**, 8930-8943.
18. M. Abed, K. Alzoubi, F. Lang and A. Al Mamun Bhuayn, *Cellular physiology and biochemistry : international journal of experimental cellular physiology, biochemistry, and pharmacology*, 2017, **41**, 543-554.
19. H. Huang, H. Shi, J. Liu, Y. Min, Y. Wang, A. Z. Wang, J. Wang and Y. Liu, *Chemical communications*, 2016, **53**, 212-215.
20. X. Li, Y. Li, X. Shen, S. Fu, S. Han and Q. Feng, *Anti-cancer drugs*, 2015, **26**, 737-746.
21. W. Yin, Y. Song, Q. Liu, Y. Wu and R. He, *Immunology*, 2017, **152**, 287-297.
22. A. Zanetti, R. Affatato, F. Centritto, M. Fratelli, M. Kurosaki, M. M. Barzago, M. Bolis, M. Terao, E. Garattini and G. Paroni, *The Journal of biological chemistry*, 2015, **290**, 17690-17709.
23. F. Cimmino, L. Pezone, M. Avitabile, G. Acierno, I. Andolfo, M. Capasso and A. Iolascon, *Scientific reports*, 2015, **5**, 11158.
24. P. Aouad, M. Saikali, R. Abdel-Samad, S. Fostok, L. El-Houjeiri, C. Pisano, R. Talhouk and N. Darwiche, *Anti-cancer drugs*, 2017, **28**, 757-770.
25. Q. Wang, Y. Guo, S. Jiang, M. Dong, K. Kuerban, J. Li, M. Feng, Y. Chen and L. Ye, *Phytomedicine*, 2017, DOI: 10.1016/j.phymed.2017.12.029.

26. K. Venkata Sairam, B. M. Gurupadayya, B. I. Vishwanathan, R. S. Chandan and D. K. Nagesha, *RSC Advances*, 2016, **6**, 98816-98828.
27. R. Z. Batran, D. H. Dawood, S. A. El-Seginy, M. M. Ali, T. J. Maher, K. S. Gugnani and A. N. Rondon-Ortiz, *Archiv der Pharmazie*, 2017, **350**.
28. Y. Zhu, J. Zhang, F. Meng, C. Deng, R. Cheng, J. Feijen and Z. Zhong, *Journal of controlled release : official journal of the Controlled Release Society*, 2016, **233**, 29-38.
29. N. He, Z. Chen, J. Yuan, L. Zhao, M. Chen, T. Wang and X. Li, *ACS applied materials & interfaces*, 2017, **9**, 32534-32544.
30. Z. Zhang, L. Shi, C. Wu, Y. Su, J. Qian, H. Deng and X. Zhu, *ACS applied materials & interfaces*, 2017, **9**, 29505-29514.
31. C. Yang, S. Huang, X. Wang and M. Wang, *Polymer Chemistry*, 2016, **7**, 7455-7468.
32. Y. Zhang, F. Huang, C. Ren, L. Yang, J. Liu, Z. Cheng, L. Chu and J. Liu, *ACS applied materials & interfaces*, 2017, **9**, 13016-13028.
33. T. C. Hsieh, C. Wong, D. John Bennett and J. M. Wu, *International journal of cancer*, 2011, **129**, 2732-2743.
34. B. Xu, Q. Jin, J. Zeng, T. Yu, Y. Chen, S. Li, D. Gong, L. He, X. Tan, L. Yang, G. He, J. Wu and X. Song, *ACS applied materials & interfaces*, 2016, **8**, 25753-25769.
35. M. Gulfam, T. Matini, P. F. Monteiro, R. Riva, H. Collins, K. Spriggs, S. M. Howdle, C. Jerome and C. Alexander, *Biomaterials science*, 2017, **5**, 532-550.
36. Z. Guo, X. Zhou, M. Xu, H. Tian, X. Chen and M. Chen, *Biomaterials science*, 2017, **5**, 2501-2510.